# Multicolor Fourier analysis of the multigrid method for quadratic FEM discretizations

C. Rodrigo*

Joint work with F.J. Gaspar and F.J. Lisbona†

**Abstract**

To design geometric multigrid methods, Local Fourier Analysis (LFA) is a very useful tool. However, LFA for quadratic finite element discretizations can not be performed in a standard way, since the discrete operator is defined by different stencils depending on the location of the points in the grid. In this work, a multicolor local Fourier analysis is presented to analyze multigrid solvers for quadratic finite element discretizations. With the help of this analysis, a four-color smoother is designed, resulting very efficient for equilateral triangular grids. By other hand, for anisotropic meshes, a zebra-line smoother is proposed. Some results showing the good correspondence between the two-grid convergence factors predicted by the analysis and the experimentally computed asymptotic convergence factors are presented.

## 1 Introduction

Finite element methods (FEM) are popular techniques for solving numerically elliptic partial differential equations (PDEs). Due to the improved approximation properties of higher order finite element methods, they are often used in practical computations. Thus, the study of fast solvers for linear systems arising from high order discretizations is meaningful.
Multigrid algorithms [2, 8] are among the most efficient methods for solving large algebraic systems arising from discretizations of PDEs. While algebraic multigrid is capable of handling large problems with irregular structure, geometric multigrid always has a lower cost per iteration.
To our knowledge, only a few references on multigrid methods for higher order finite elements, most of them related to algebraic multigrid, are found in the literature, see e.g. [4, 7]. In the context of geometric multigrid methods, a numerical analysis of quadratic FEM is discussed in [5]. However, quantitative estimates of the convergence of geometric multigrid methods, in function of the chosen components, are missing in the literature. This question is at the focus of this paper.

Local Fourier analysis (LFA), introduced by A. Brandt [1], is the most powerful tool for the quantitative analysis and design of efficient geometric multigrid methods for general problems. From a practical point of view, LFA is helpful because it provides realistic quantitative estimates of the asymptotic multigrid convergence factor, see [8, 9]. However, local Fourier analysis cannot be directly applied to high-order discretization operators because different stencils appear depending on the location of the nodes. To overcome this trouble, a multicolor local Fourier analysis is introduced, which in some sense generalizes the two-color Fourier analysis presented in [6]. In this

*Centro Universitario de la Defensa. Academia General Militar. Ctra. Huesca s/n, 50090 Zaragoza, Spain. E-mail: carmenr@unizar.es

†Department of Applied Mathematics, University of Zaragoza, Pedro Cerbuna 12, 50009 Zaragoza, Spain

paper, this analysis is presented for quadratic finite element methods, but in principle, it is possible to extend the main idea to more general high-order elements.

For simplicity in the presentation, we shall consider the Poisson equation as model problem, since it results in the standard benchmark problem for studying the performance of linear solvers:

$$-\Delta u = f, \text{ in } \Omega.$$

We also consider the corresponding algebraic linear system arising from its discretization by quadratic FEM: $L_h u_h = f_h$, associated with a triangular partition $\mathcal{T}_h$ of the domain $\Omega$.

The organization of the paper is as follows. Section 2 is devoted to the presentation of the multicolor smoothing local Fourier analysis on a triangular grid associated with a Cartesian grid. The corresponding multicolor two-grid Fourier analysis is introduced in Section 3. Some Fourier results are displayed in Section 4 and confirmed by some numerical computations. In Section 5, the multicolor Fourier analysis is extended to more general regular triangulations.

## 2 Multicolor smoothing Fourier analysis

A multicolor local Fourier analysis is presented to analyze the smoothing properties of relaxation methods for quadratic finite element discretizations. This analysis exploits the *periodicity* of the stencils and it can be seen as an extension of the two-color Fourier analysis introduced by C.-C.J. Kuo and B.C. Levy in [6].
Despite the fact that different stencils result from the discretization by quadratic FEM, those associated with grid-points of the same type are identical. As we will see, this fact permits to develop a local Fourier analysis. In the particular case of isosceles rectangular triangular grids, see right Figure 1, we distinguish four different types of points, called type (a), (b), (c) and (d), see left Figure 1, for which the corresponding stencils are displayed in Figure 2.

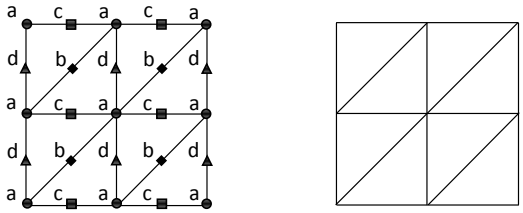


Figure 1: Different types of nodes on a rectangular triangular grid.

To perform the analysis, the infinite grid: $\Omega_h = \{\mathbf{x} = (x_1, x_2) \in \mathbb{R}^2 | \, x_i = k_i h, \, k_i \in \mathbb{Z}, \, i = 1, 2\}$ is split into four different types of grids, each one associated with a different color:

$$\begin{aligned} \Omega_h^{00} &= \{(k_1 h, k_2 h) \in \Omega_h | \, k_1 \text{ even}, \; k_2 \text{ even}\}, \qquad \Omega_h^{11} = \{(k_1 h, k_2 h) \in \Omega_h | \, k_1 \text{ odd}, \; k_2 \text{ odd}\}, \\ \Omega_h^{10} &= \{(k_1 h, k_2 h) \in \Omega_h | \, k_1 \text{ odd}, \; k_2 \text{ even}\}, \qquad \Omega_h^{01} = \{(k_1 h, k_2 h) \in \Omega_h | \, k_1 \text{ even}, \; k_2 \text{ odd}\}. \end{aligned} \tag{1}$$

The subgrids $\Omega_h^{00}$, $\Omega_h^{11}$, $\Omega_h^{10}$, and $\Omega_h^{01}$ correspond to the extension to infinite grids of the subdivision of the computational grid in points of type (a), (b), (c) and (d), respectively. Note that all grid-points of an specific subgrid $\Omega_h^{kl}$ have the same stencil.

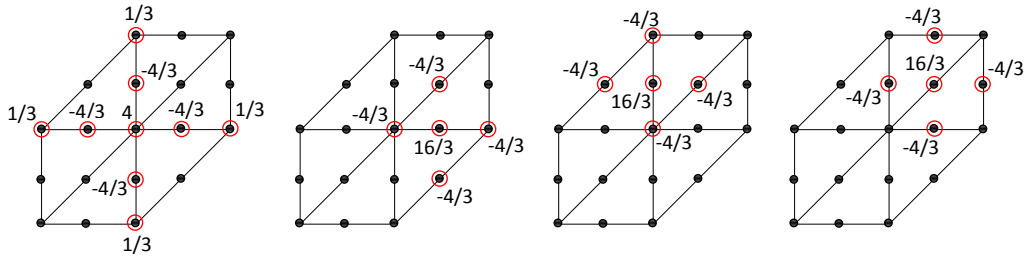


type (a) type (c) type (d) type (b)

Figure 2: Stencils for quadratic FEM discretization of the Laplace operator on a rectangular triangular grid.

For each low-frequency $\boldsymbol{\theta}^{00} \in \boldsymbol{\Theta}_{2h} = (-\pi/2h,\, \pi/2h]^2$, and taking into account the corresponding Fourier mode $\varphi_h(\boldsymbol{\theta}^{00}, \mathbf{x}) = e^{i\boldsymbol{\theta}^{00}\cdot\mathbf{x}}$, let us introduce the following grid-functions:

$$\psi_h^{kl}(\boldsymbol{\theta}^{00}, \mathbf{x}) = \varphi_h(\boldsymbol{\theta}^{00}, \mathbf{x})\chi_{\Omega_h^{kl}}(\mathbf{x}), \quad k, l = 0, 1,\ \mathbf{x} \in \Omega_h. \tag{2}$$

Due to the following relations

$$\begin{pmatrix} \psi_h^{00}(\boldsymbol{\theta}^{00}, \cdot) \\ \psi_h^{11}(\boldsymbol{\theta}^{00}, \cdot) \\ \psi_h^{10}(\boldsymbol{\theta}^{00}, \cdot) \\ \psi_h^{01}(\boldsymbol{\theta}^{00}, \cdot) \end{pmatrix} = M \begin{pmatrix} \varphi_h(\boldsymbol{\theta}^{00}, \cdot) \\ \varphi_h(\boldsymbol{\theta}^{11}, \cdot) \\ \varphi_h(\boldsymbol{\theta}^{10}, \cdot) \\ \varphi_h(\boldsymbol{\theta}^{01}, \cdot) \end{pmatrix} = \frac{1}{4} \begin{pmatrix} 1 & 1 & 1 & 1 \\ 1 & 1 & -1 & -1 \\ 1 & -1 & -1 & 1 \\ 1 & -1 & 1 & -1 \end{pmatrix} \begin{pmatrix} \varphi_h(\boldsymbol{\theta}^{00}, \cdot) \\ \varphi_h(\boldsymbol{\theta}^{11}, \cdot) \\ \varphi_h(\boldsymbol{\theta}^{10}, \cdot) \\ \varphi_h(\boldsymbol{\theta}^{01}, \cdot) \end{pmatrix}, \tag{3}$$

where $\varphi_h(\boldsymbol{\theta}^{kl}, \cdot)$, with $\boldsymbol{\theta}^{kl} = \boldsymbol{\theta}^{00} - \left(k\,\mathrm{sign}(\theta_1^{00}), l\,\mathrm{sign}(\theta_2^{00})\right)\pi/h$, $k, l = 0, 1$, generate the subspaces of $2h-$harmonics:

$$\mathcal{F}_h^4(\boldsymbol{\theta}^{00}) = span\{\varphi_h(\boldsymbol{\theta}^{00}, \cdot), \varphi_h(\boldsymbol{\theta}^{11}, \cdot), \varphi_h(\boldsymbol{\theta}^{10}, \cdot), \varphi_h(\boldsymbol{\theta}^{01}, \cdot)\}, \quad \boldsymbol{\theta}^{00} \in \boldsymbol{\Theta}_{2h}, \tag{4}$$

it is immediate that these subspaces can be also written as

$$\mathcal{F}_h^4(\boldsymbol{\theta}^{00}) = span\{\psi_h^{00}(\boldsymbol{\theta}^{00}, \cdot), \psi_h^{11}(\boldsymbol{\theta}^{00}, \cdot), \psi_h^{10}(\boldsymbol{\theta}^{00}, \cdot), \psi_h^{01}(\boldsymbol{\theta}^{00}, \cdot)\}, \quad \boldsymbol{\theta}^{00} \in \boldsymbol{\Theta}_{2h}. \tag{5}$$

**Proposition 2.1.** *Discrete operator $L_h$ leaves subspaces $\mathcal{F}_h^4(\boldsymbol{\theta}^{00})$ invariant.*

*Proof.* In order to demonstrate this invariance property, $L_h : \mathcal{F}_h^4(\boldsymbol{\theta}^{00}) \to \mathcal{F}_h^4(\boldsymbol{\theta}^{00})$, we use grid-functions $\{\psi_h^{kl}\}_{k,l=0,1}$, introduced in (2). We must show that the application of operator $L_h$ to these grid-functions can be written as a linear combination of themselves. More concretely, we have to find coefficients $c_{nm}^{kl}$, $k, l, n, m = 0, 1$, such that for all $\mathbf{x} \in \Omega_h$,

$$(L_h\psi_h^{kl})(\boldsymbol{\theta}^{00}, \mathbf{x}) = c_{00}^{kl}\psi_h^{00}(\boldsymbol{\theta}^{00}, \mathbf{x}) + c_{11}^{kl}\psi_h^{11}(\boldsymbol{\theta}^{00}, \mathbf{x}) + c_{10}^{kl}\psi_h^{10}(\boldsymbol{\theta}^{00}, \mathbf{x}) + c_{01}^{kl}\psi_h^{01}(\boldsymbol{\theta}^{00}, \mathbf{x}). \tag{6}$$

In order to compute these coefficients, expression (6) is evaluated in the four different kind of grids $\Omega_h^{kl}$, $k, l = 0, 1$. For example, for $\psi_h^{00}(\boldsymbol{\theta}^{00}, \mathbf{x})$, this evaluation gives rise to the following equations:

$$\begin{aligned}
\mathbf{x} \in \Omega_h^{00}: \quad & 4\varphi_h(\boldsymbol{\theta}^{00}, \mathbf{x}) + \frac{1}{3}\left[\varphi_h(\boldsymbol{\theta}^{00}, (x_1 + 2h, x_2)) + \varphi_h(\boldsymbol{\theta}^{00}, (x_1 - 2h, x_2))\right. \\
& \left. + \varphi_h(\boldsymbol{\theta}^{00}, (x_1, x_2 + 2h)) + \varphi_h(\boldsymbol{\theta}^{00}, (x_1, x_2 - 2h))\right] = c_{00}^{00}\varphi_h(\boldsymbol{\theta}^{00}, \mathbf{x}), \\
\mathbf{x} \in \Omega_h^{11}: \quad & 0 = c_{11}^{00}\varphi_h(\boldsymbol{\theta}^{00}, \mathbf{x}), \\
\mathbf{x} \in \Omega_h^{10}: \quad & -\frac{4}{3}\left[\varphi_h(\boldsymbol{\theta}^{00}, (x_1 + h, x_2)) + \varphi_h(\boldsymbol{\theta}^{00}, (x_1 - h, x_2))\right] = c_{10}^{00}\varphi_h(\boldsymbol{\theta}^{00}, \mathbf{x}), \\
\mathbf{x} \in \Omega_h^{01}: \quad & -\frac{4}{3}\left[\varphi_h(\boldsymbol{\theta}^{00}, (x_1, x_2 + h)) + \varphi_h(\boldsymbol{\theta}^{00}, (x_1, x_2 - h))\right] = c_{01}^{00}\varphi_h(\boldsymbol{\theta}^{00}, \mathbf{x}),
\end{aligned}$$

and from these expressions the values of coefficients $c_{nm}^{00},\ n,m=0,1$, result in

$$c_{00}^{00}=4+\frac{2}{3}\left(\cos(2\theta_1^{00}h)+\cos(2\theta_2^{00}h)\right),\quad c_{11}^{00}=0,\quad c_{10}^{00}=-\frac{8}{3}\cos(\theta_1^{00}h),\quad c_{01}^{00}=-\frac{8}{3}\cos(\theta_2^{00}h).$$

Similar computations can be done to calculate the rest of the coefficients, and they give rise to

$$\begin{pmatrix}(L_h\psi_h^{00})(\boldsymbol{\theta}^{00},\cdot)\\(L_h\psi_h^{11})(\boldsymbol{\theta}^{00},\cdot)\\(L_h\psi_h^{10})(\boldsymbol{\theta}^{00},\cdot)\\(L_h\psi_h^{01})(\boldsymbol{\theta}^{00},\cdot)\end{pmatrix}=\widehat{L}_h(\boldsymbol{\theta}^{00})\begin{pmatrix}\psi_h^{00}(\boldsymbol{\theta}^{00},\cdot)\\\psi_h^{11}(\boldsymbol{\theta}^{00},\cdot)\\\psi_h^{10}(\boldsymbol{\theta}^{00},\cdot)\\\psi_h^{01}(\boldsymbol{\theta}^{00},\cdot)\end{pmatrix},$$

where $\widehat{L}_h(\boldsymbol{\theta}^{00})$ is the Fourier symbol or Fourier representation of operator $L_h$ in subspace $\mathcal{F}_h^4(\boldsymbol{\theta}^{00})$, with respect to functions given in (2). □

*Remark 1.* From Proposition 2.1, the discrete operator associated with quadratic FEM leaves invariant the spaces of $2h-$harmonics, being the only difference with discretizations given by only one stencil, that the symbol $\widehat{L}_h(\boldsymbol{\theta}^{00})$ results in a full $4\times 4-$matrix. The same occurs with the symbol of any smoothing operator $S_h$ based on a decomposition of the discrete operator $L_h=L_h^+ + L_h^-$.

*Remark 2.* One can obtain the symbol of the discrete operator $L_h$ with respect to the grid-functions $\{\varphi_h(\boldsymbol{\theta}^{kl},\cdot)\}_{k,l=0,1}$, by using the expression $M\widehat{L}_h(\boldsymbol{\theta}^{00})M^{-1}$, where $M$ is given in (3).

Finally, given a smoothing operator $S_h$ and taking into account *Remark 2* applied to $S_h$, we can define the smoothing factor per sweep, for $\nu$ consecutive sweeps, as

$$\mu(S_h,\nu)=\sup_{\boldsymbol{\theta}^{00}\in\boldsymbol{\Theta}_{2h}}\sqrt[\nu]{\rho(\widehat{Q}(\boldsymbol{\theta}^{00})M\widehat{S}_h^{\nu}(\boldsymbol{\theta}^{00})M^{-1})},\quad\text{where }\widehat{Q}(\boldsymbol{\theta}^{00})=\begin{pmatrix}0&&&\\&1&&\\&&1&\\&&&1\end{pmatrix}.\qquad(7)$$

## 2.1 Four-color smoother and its multicolor smoothing Fourier analysis

Here we propose a four-color smoother, which consists of splitting the original grid into four subsets, as in (1), and performing successively a Jacobi sweep on each one of these subgrids. This results in an expression of this smoother $S_h$ as a composition of partial smoothing step operators in the following way $S_h=S_h^{01}S_h^{11}S_h^{10}S_h^{00}$, where

$$S_h^{kl}\psi_h(\mathbf{x})=\begin{cases}[(I_h-\omega_{kl}D_h^{-1}L_h)\psi_h](\mathbf{x}), & \mathbf{x}\in\Omega_h^{kl},\\ \psi_h(\mathbf{x}), & \mathbf{x}\in\Omega_h\backslash\Omega_h^{kl},\end{cases}\qquad k,l=0,1,\qquad(8)$$

where $D_h$ denotes the diagonal part of $L_h$, and $\omega_{kl},\ k,l=0,1$, are relaxation parameters, which can be chosen to be different for each one of the four partial smoothing step operators.

**Proposition 2.2.** *Four-color smoothing operator $S_h$ leaves spaces $\mathcal{F}_h^4(\boldsymbol{\theta}^{00})$ invariant.*

*Proof.* This result comes from the fact that each of the four partial smoothing step operators $S_h^{kl},\ k,l=0,1$, defined in (8), also fulfills this invariance property. This can be demonstrated similarly as Proposition 2.1, by using the grid-functions $\{\psi_h^{kl}\}_{k,l=0,1}$. That is, writing $S_h^{nm}\psi_h^{kl}(\boldsymbol{\theta}^{00},\mathbf{x})$ as a linear combination of the four grid-functions $\psi_h^{kl}(\boldsymbol{\theta}^{00},\mathbf{x})$ generating subspace $\mathcal{F}_h^4(\boldsymbol{\theta}^{00})$, for each $S_h^{nm}$ with $n,m=0,1$. □

From the proof of previous proposition, we can obtain the Fourier representation of $S_h$ in $\mathcal{F}_h^4(\boldsymbol{\theta}^{00})$, with respect to grid-functions $\{\psi_h^{kl}\}_{k,l=0,1}$, denoted by $\widehat{S}_h$, and the smoothing factor corresponding to this relaxation scheme can be computed using formula (7).

# 3 Multicolor two-grid Fourier analysis

At least a two-grid Fourier analysis is necessary to analyze the interplay between the smoother and the coarse-grid correction. This analysis accurately predicts the asymptotic convergence factor of a two-grid method, $K_h^{2h}$, which is given by $K_h^{2h} = S_h^{\nu_2} C_h S_h^{\nu_1} = S_h^{\nu_2}(I_h - P_{2h}^h L_{2h}^{-1} R_h^{2h} L_h) S_h^{\nu_1}$, where $S_h$ is a relaxation operator, and $C_h$ is the coarse-grid correction operator, composed of the inter-grid transfer operators: $R_h^{2h}$, $P_{2h}^h$, restriction and prolongation respectively, and the discrete operators $L_h$, $L_{2h}$, on the fine and coarse grids respectively.
As commented for the smoothing Fourier analysis, a "standard" two-grid analysis cannot be applied when quadratic finite element discretizations are considered. Thus, a multicolor two-grid LFA is introduced in this section in order to deal with this type of discretizations. In order to perform such analysis, the original infinite grid is split into sixteen different subgrids, defined as follows

$$\Omega_h^{kl} = \{(4k_1, 4k_2)h + (k,l)h |\ k_1, k_2 \in \mathbb{Z}\}, \quad k,l = 0,\ldots,3. \tag{9}$$

Given $\boldsymbol{\theta}^{00} = \boldsymbol{\theta}_{00}^{00} \in \boldsymbol{\Theta}_{4h} = (-\pi/4h, \pi/4h]^2$, we introduce the following grid-functions:

$$\psi_h^{kl}(\boldsymbol{\theta}^{00}, \mathbf{x}) = \varphi_h(\boldsymbol{\theta}^{00}, \mathbf{x}) \chi_{\Omega_h^{kl}}(\mathbf{x}), \quad k,l = 0,\ldots,3,\ \mathbf{x} \in \Omega_h. \tag{10}$$

Thus, the following $16-$dimensional subspaces are considered

$$\mathcal{F}_h^{16}(\boldsymbol{\theta}^{00}) = span\{\psi_h^{kl}(\boldsymbol{\theta}^{00}, \cdot),\ k,l = 0,\ldots,3\}. \tag{11}$$

These subspaces can be written in function of four subsets of $2h-$harmonics in the following way

$$\mathcal{F}_h^{16}(\boldsymbol{\theta}^{00}) = span\{\varphi_h(\boldsymbol{\theta}_{nm}^{ij}, \cdot),\ i,j,n,m = 0,1\},$$

where

$$\begin{aligned} \boldsymbol{\theta}_{nm}^{00} &= \boldsymbol{\theta}_{00}^{00} - (n\pi\, sign(\theta_1^{00})/2h, m\pi\, sign(\theta_2^{00})/2h) \\ \boldsymbol{\theta}_{nm}^{ij} &= \boldsymbol{\theta}_{nm}^{00} - (i\pi\, sign((\theta_{nm}^{00})_1)/h, j\pi\, sign((\theta_{nm}^{00})_2)/h), \end{aligned}$$

are frequencies depicted in Figure 3, which are just those coupled frequencies in a three-grid Fourier analysis, see [9]. In fact, the following relation between the grid-functions $\{\varphi_h(\boldsymbol{\theta}_{nm}^{ij}, \cdot)\}_{i,j,n,m=0,1}$ and $\{\psi_h^{kl}\}_{k,l=0,\ldots,3}$ is fulfilled: $(\boldsymbol{\psi}) = \mathbb{M}(\boldsymbol{\varphi})$, where $(\boldsymbol{\psi})$ and $(\boldsymbol{\varphi})$ are given by the following vectors of grid-functions:

$$\left(\psi_h^{00}, \psi_h^{11}, \psi_h^{10}, \psi_h^{01}, \psi_h^{22}, \psi_h^{33}, \psi_h^{32}, \psi_h^{23}, \psi_h^{20}, \psi_h^{31}, \psi_h^{30}, \psi_h^{21}, \psi_h^{02}, \psi_h^{13}, \psi_h^{12}, \psi_h^{03}\right)^t,$$

and

$$\begin{aligned} &\big(\varphi_h(\boldsymbol{\theta}_{00}^{00}, \cdot), \varphi_h(\boldsymbol{\theta}_{00}^{11}, \cdot), \varphi_h(\boldsymbol{\theta}_{00}^{10}, \cdot), \varphi_h(\boldsymbol{\theta}_{00}^{01}, \cdot), \varphi_h(\boldsymbol{\theta}_{11}^{00}, \cdot), \varphi_h(\boldsymbol{\theta}_{11}^{11}, \cdot), \varphi_h(\boldsymbol{\theta}_{11}^{10}, \cdot), \varphi_h(\boldsymbol{\theta}_{11}^{01}, \cdot), \\ &\varphi_h(\boldsymbol{\theta}_{10}^{00}, \cdot), \varphi_h(\boldsymbol{\theta}_{10}^{11}, \cdot), \varphi_h(\boldsymbol{\theta}_{10}^{10}, \cdot), \varphi_h(\boldsymbol{\theta}_{10}^{01}, \cdot), \varphi_h(\boldsymbol{\theta}_{01}^{00}, \cdot), \varphi_h(\boldsymbol{\theta}_{01}^{11}, \cdot), \varphi_h(\boldsymbol{\theta}_{01}^{10}, \cdot), \varphi_h(\boldsymbol{\theta}_{01}^{01}, \cdot)\big)^t, \end{aligned}$$

respectively, and matrix $\mathbb{M}$ is the Kronecker product $M \otimes M$, i.e.

$$\mathbb{M} = \frac{1}{4} \begin{pmatrix} M & M & M & M \\ M & M & -M & -M \\ M & -M & -M & M \\ M & -M & M & -M \end{pmatrix}. \tag{12}$$

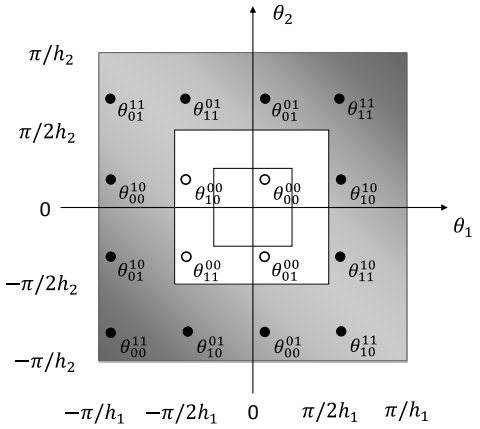


Figure 3: Sixteen frequencies generating $\mathcal{F}_h^{16}(\boldsymbol{\theta}_{00}^{00})$.

Due to this relation and taking into account Propositions 2.1 and 2.2, it is immediate that discrete operator $L_h$, as well as any smoothing operator $S_h$, including four-color relaxation, leaves invariant subspaces $\mathcal{F}_h^{16}(\boldsymbol{\theta}^{00})$. Thus, Fourier representation of such operators with respect to grid-functions $\{\psi_h^{kl}\}_{k,l=0,\ldots,3}$ can be computed in a similar way to that done in Proposition 2.1.

**Proposition 3.1.** *The coarse-grid correction operator, $C_h$, leaves subspaces $\mathcal{F}_h^{16}(\boldsymbol{\theta}^{00})$ invariant.*

*Proof.* The proof of this fact is based on the following properties of the operators involved in $C_h$ :

(a) $L_h$, $I_h : \mathcal{F}_h^{16}(\boldsymbol{\theta}^{00}) \to \mathcal{F}_h^{16}(\boldsymbol{\theta}^{00})$,

(b) $L_{2h} : \mathcal{F}_{2h}^{4}(2\boldsymbol{\theta}^{00}) \to \mathcal{F}_{2h}^{4}(2\boldsymbol{\theta}^{00})$,

(c) $P_{2h}^{h} : \mathcal{F}_{2h}^{4}(2\boldsymbol{\theta}^{00}) \to \mathcal{F}_h^{16}(\boldsymbol{\theta}^{00})$, and $R_h^{2h} : \mathcal{F}_h^{16}(\boldsymbol{\theta}^{00}) \to \mathcal{F}_{2h}^{4}(2\boldsymbol{\theta}^{00})$,

where subspaces $\mathcal{F}_{2h}^{4}(2\boldsymbol{\theta}^{00})$ are given as in (4), on the coarse grid $\Omega_{2h}$ and with $\boldsymbol{\theta}^{00} \in \boldsymbol{\Theta}_{4h}$.
Property (a) has been already commented above, and the invariance property of operator $L_{2h}$ in (b) follows from direct application of Proposition 2.1 considering $\Omega_{2h}$.
With respect to prolongation operator, it is possible to demonstrate (c) for many different types of interpolations, in particular for quadratic, which is considered in this work. In order to see that, the mechanism is similar to that applied in the proof of the invariance property of the discrete operator $L_h$ in Proposition 2.1. More concretely, the invariance is proved by writing

$$(P_{2h}^{h}\psi_{2h}^{kl}(\boldsymbol{\theta}^{00},\cdot))(\mathbf{x}) = \sum_{n,m=0}^{3} c_{nm}^{kl}\psi_h^{nm}(\boldsymbol{\theta}^{00},\mathbf{x}), \quad k,l=0,1,$$

and determining constants $c_{nm}^{kl}$ by evaluating the above expression on each subgrid $\Omega_h^{nm}$, $n,m = 0,\ldots,3$. In this way, we obtain the matrix representation of the prolongation operator $P_{2h}^{h}$ with respect to grid-functions $\{\psi_{2h}^{kl}\}_{k,l=0,1}$ and $\{\psi_h^{nm}\}_{n,m=0,\ldots,3}$. Finally, by considering the adjoint of the interpolation as the restriction operator, it is immediate the invariance property given in (c) for $R_h^{2h}$. The corresponding representation matrix $\widehat{R}_h^{2h}(\boldsymbol{\theta}^{00})$ can be calculated as $\widehat{R}_h^{2h}(\boldsymbol{\theta}^{00}) = \dfrac{1}{4}(\widehat{P}_{2h}^{h}(\boldsymbol{\theta}^{00}))^*$. □

As an immediate consequence, the two-grid operator, $K_h^{2h}$, leaves subspaces $\mathcal{F}_h^{16}(\boldsymbol{\theta}^{00})$ invariant, and its representation matrix with respect to $\{\psi_h^{nm}\}_{n,m=0,\ldots,3}$ is $\widehat{K}_h^{2h}(\boldsymbol{\theta}^{00}) = \widehat{S}_h^{\nu_2}(\boldsymbol{\theta}^{00})\widehat{C}_h(\boldsymbol{\theta}^{00})\widehat{S}_h^{\nu_1}(\boldsymbol{\theta}^{00})$,

with $\widehat{C}_h(\boldsymbol{\theta}^{00}) = \widehat{I}_h(\boldsymbol{\theta}^{00}) - \widehat{P}_{2h}^h(\boldsymbol{\theta}^{00})(\widehat{L}_{2h}(2\boldsymbol{\theta}^{00}))^{-1}\widehat{R}_h^{2h}(\boldsymbol{\theta}^{00})\widehat{L}_h(\boldsymbol{\theta}^{00})$.
Finally, the asymptotic two-grid convergence factor can be computed as the supremum of the spectral radii of $16 \times 16-$matrices $\widehat{K}_h^{2h}(\boldsymbol{\theta}^{00})$, i.e. $\rho(K_h^{2h}) = \sup_{\boldsymbol{\theta}^{00} \in \widetilde{\boldsymbol{\Theta}}_{4h}} \rho(\widehat{K}_h^{2h}(\boldsymbol{\theta}^{00}))$, where $\widetilde{\boldsymbol{\Theta}}_{4h}$ is the subset of $\boldsymbol{\Theta}_{4h}$ in which we remove the frequencies $\boldsymbol{\theta}^{00} \in \boldsymbol{\Theta}_{4h}$ such that the Fourier symbols of $L_h$, $L_{2h}$, or $L_{4h}$ vanish.

# 4 Multicolor local Fourier analysis results

In this section we present some results obtained by the previously introduced multicolor LFA. To this end, several point-wise as well as line-wise smoothers are considered. First, standard damped Jacobi and lexicographic Gauss-Seidel schemes are compared to the four-color smoother introduced in Section 2.1. In the case of Jacobi relaxation, we have used the optimal parameter $\omega = 0.75$, which has been seen to be optimal from the multicolor LFA. The ordering used for the four-color smoother has been chosen as follows: first unknowns of type (a) are updated, then those with type (c) are relaxed, next nodes type (b) and finally those type (d) are visited, see Figure 1. This ordering is chosen because we have observed from the analysis that it results in one of the best convergence rates between the possible combinations.
In Table 1, we show the smoothing factors, $\mu^\nu$, and the two-grid convergence factors, $\rho$, for different numbers of smoothing steps, $\nu$, for quadratic interpolation and its adjoint for the restriction. We also display in this table the experimentally measured W-cycle convergence factors (denoted by $\rho_h$) using eight levels of refinement, obtained with a random initial guess and a zero right-hand side to avoid round-off errors.
From this table, we can see that the convergence factors are very well-predicted by this multicolor LFA in all cases. Moreover, we also observe that the four-color smoother, proposed here, provides the best convergence factors among the three considered point-wise smoothers. The behavior of this smoother will be much better when equilateral triangular grids are considered, as will be seen in Section 5.

| | Damped Jacobi | | | Gauss-Seidel | | | Four-color | | |
|---|---|---|---|---|---|---|---|---|---|
| $\nu$ | $\mu^\nu$ | $\rho$ | $\rho_h$ | $\mu^\nu$ | $\rho$ | $\rho_h$ | $\mu^\nu$ | $\rho$ | $\rho_h$ |
| 1 | 0.654 | 0.631 | 0.635 | 0.544 | 0.559 | 0.554 | 0.289 | 0.323 | 0.324 |
| 2 | 0.428 | 0.481 | 0.480 | 0.296 | 0.340 | 0.335 | 0.084 | 0.204 | 0.203 |
| 3 | 0.279 | 0.379 | 0.379 | 0.161 | 0.212 | 0.210 | 0.024 | 0.132 | 0.131 |
| 4 | 0.183 | 0.312 | 0.311 | 0.088 | 0.139 | 0.140 | 0.007 | 0.079 | 0.079 |

Table 1: Multicolor LFA smoothing factors, $\mu^\nu$, two–grid convergence factors, $\rho$, and measured $W-$cycle convergence rates $\rho_h$, for different point-wise smoothers and for different numbers of smoothing steps, $\nu$.

Next, in Table 2, the results obtained with two different line smoothers: a simple lexicographic line-wise Gauss-Seidel and the zebra-line smoother, for quadratic interpolation, are shown. The considered zebra-line smoother consists of a first step relaxing simultaneously all unknowns on lines composed of type (a) and (c) nodes, and then a second step updating the rest of the lines where type (b) and (d) nodes are located. Again, a very good correspondence between the theoretical and practical convergence rates is observed in all cases. Besides, we want to claim the exceptional results provided by zebra-line smoother, which reduces by almost a half the convergence factors corresponding to the lexicographic line-wise Gauss-Seidel.

| | Lex. line smoother | | Zebra-line smoother | |
|---|---|---|---|---|
| $\nu$ | $\rho$ | $\rho_h$ | $\rho$ | $\rho_h$ |
| 1 | 0.395 | 0.390 | 0.250 | 0.250 |
| 2 | 0.179 | 0.176 | 0.084 | 0.083 |
| 3 | 0.116 | 0.112 | 0.030 | 0.029 |
| 4 | 0.053 | 0.052 | 0.016 | 0.016 |

Table 2: Multicolor LFA two–grid convergence factors, $\rho$, and measured $W$–cycle convergence rates, $\rho_h$, for different line-wise smoothers and different numbers of smoothing steps, $\nu$.

# 5 Extension of multicolor LFA to more general structured triangulations

Here, we extend the multicolor local Fourier analysis to any structured triangular grid characterized by two angles $\alpha$ and $\beta$, see right Figure 4. Standard LFA for multigrid methods on these types of meshes was recently introduced in [3] for linear finite element methods. This analysis is based on an expression of the Fourier transform in new coordinate systems in space and frequency variables. More concretely, a unitary basis of $\mathbb{R}^2$, $\{\mathbf{e}_1', \mathbf{e}_2'\}$, fitting the geometry of the mesh (see right Figure 4), is considered, and its reciprocal basis is taken for the frequency space. This fact makes that the LFA on general triangular grids is straightforward from that on rectangular grids. Anyway, for quadratic FEM on structured triangular grids, this analysis cannot be applied because of the same reasons pointed out for the previously considered rectangular triangular grids. Therefore, a multicolor LFA is necessary to deal with this type of discretizations on general structured triangular grids. In order to perform this analysis, those reciprocal bases, commented above, have to be taken into account.

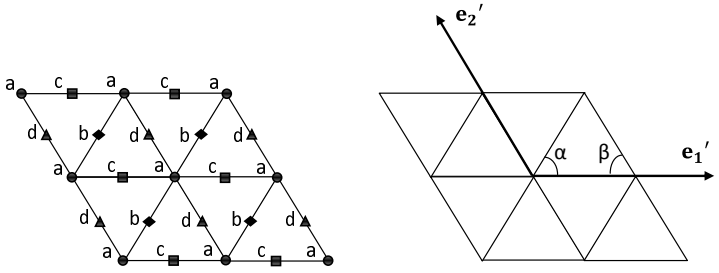


Figure 4: Different types of nodes on a general triangular grid, characterized by angles $\alpha$ and $\beta$.

The special smoothers proposed in this work for quadratic FEM on rectangular triangular grids, can be generalized to any structured triangulation. With this purpose, again we split the grid into four different types of nodes: (a), (b), (c) and (d), see left Figure 4. Then, the four-color smoother relax nodes of type (a), (c), (b), (d), in this order. Three different zebra-line smoothers can also be considered, related to the lines parallel to the opposite edge to each vertex. These smoothers consist of relaxing simultaneously first all the unknowns located at lines where the vertexes are situated, and then the rest of the lines.

The quadratic FEM discretization on this regular structured grid, in principle, can be represented by four stencils corresponding to the different types of nodes. However, the stencils associated with the mid points of the edges have the same form. An expression of such stencils in function of the two angles characterizing the grid can be obtained. The corresponding stencil for

the vertexes results

$$\frac{1}{3}\begin{bmatrix} 0 & 0 & r(r+s) & 0 & s(r+s) \\ 0 & 0 & -4r(r+s) & -4s(r+s) & 0 \\ 1-rs & 4(rs-1) & 6(r^2+s^2+rs+1) & 4(rs-1) & 1-rs \\ 0 & -4s(r+s) & -4r(r+s) & 0 & 0 \\ s(r+s) & 0 & r(r+s) & 0 & 0 \end{bmatrix}, \tag{13}$$

where $r = \cot(\alpha)$ and $s = \cot(\beta)$. For the mid points of the edges the stencil reads

$$\frac{4}{3}\begin{bmatrix} 0 & -r(r+s) & -s(r+s) \\ rs-1 & 2(r^2+s^2+rs+1) & rs-1 \\ -s(r+s) & -r(r+s) & 0 \end{bmatrix}. \tag{14}$$

As an example, the stencils corresponding to an equilateral triangular grid are depicted in Figure 5.

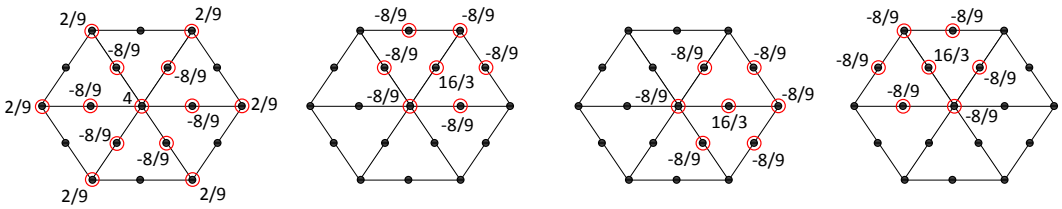


type (a) type (b) type (c) type (d)

Figure 5: Stencils for quadratic FEM discretization of the Laplace operator for equilateral triangular grids.

This expression of the stencils in function of the angles allows us to investigate the influence of the shape of the mesh on the obtained multigrid convergence. To this end, we begin comparing the behavior of some point-wise smoothers on an equilateral triangular grid. Jacobi, damped Jacobi with optimal relaxation parameter $\omega = 0.9$, a lexicographic Gauss-Seidel and the four-color smoother previously introduced are considered. In Table 3, the two-grid convergence factors predicted by the multicolor LFA are shown together with the experimentally computed asymptotic convergence factors, for different numbers of smoothing steps. From this table, it yields that the multicolor local Fourier analysis predicts very well the asymptotic two-grid convergence factors for general structured triangular grids. Besides, an excellent performance for the four-color smoother is observed, since with only two smoothing steps an asymptotic convergence factor about 0.06 is obtained, resulting this smoother in a very satisfactory relaxation scheme for the quadratic FEM discretization of model problem (1), when equilateral triangulations are considered.

| | Undamped Jacobi | | Damped Jacobi | | Gauss-Seidel | | Four-color | |
|---|---|---|---|---|---|---|---|---|
| $\nu$ | $\rho$ | $\rho_h$ | $\rho$ | $\rho_h$ | $\rho$ | $\rho_h$ | $\rho$ | $\rho_h$ |
| 1 | 0.493 | 0.492 | 0.399 | 0.399 | 0.379 | 0.380 | 0.158 | 0.157 |
| 2 | 0.382 | 0.386 | 0.252 | 0.252 | 0.160 | 0.158 | 0.058 | 0.058 |
| 3 | 0.202 | 0.207 | 0.103 | 0.103 | 0.075 | 0.072 | 0.029 | 0.029 |
| 4 | 0.157 | 0.158 | 0.078 | 0.078 | 0.045 | 0.043 | 0.016 | 0.016 |

Table 3: Multicolor LFA two–grid convergence factors, $\rho$, and measured $W$–cycle convergence rates $\rho_h$, for different point-wise smoothers and for different numbers of smoothing steps, $\nu$, on equilateral triangular grids.

As expected, the highly satisfactory factors of the four-color smoother obtained for equilateral triangular grids worsen when anisotropic triangular meshes are dealt with. For instance, a very poor convergence factor about 0.9 is obtained by this smoother when a structured triangular grid composed of isosceles triangles with common angle $85^{\mathrm{O}}$ is considered. In these cases, line-wise smoothers are required. In Table 4, results for both lexicographic and zebra-line smoothers, corresponding to the smallest angle, are shown. An excellent behavior of zebra-line smoother, with a convergence factor close to 0.1, is obtained with only one smoothing step. Note the big difference in the performance between both types of line smoothers.

| | Lex. line smoother | | Zebra-line smoother | |
|---|---|---|---|---|
| $\nu$ | $\rho$ | $\rho_h$ | $\rho$ | $\rho_h$ |
| 1 | 0.353 | 0.360 | 0.114 | 0.113 |
| 2 | 0.129 | 0.126 | 0.043 | 0.043 |
| 3 | 0.112 | 0.110 | 0.026 | 0.027 |
| 4 | 0.032 | 0.035 | 0.019 | 0.019 |

Table 4: Multicolor LFA two–grid convergence factors, $\rho$, and measured $W$–cycle convergence rates $\rho_h$, for different smoothers and numbers of smoothing steps, $\nu$, on an isosceles triangular grid with common angle $85^{\mathrm{O}}$.

As conclusion of this work, we can say that the multicolor local Fourier analysis is a very useful tool to design efficient geometric multigrid methods for quadratic finite element discretizations.

# References


[1] A. Brandt. *Multi-level adaptive solutions to boundary-value problems.* Math. Comput., 31 (1977), pp. 333–390.

[2] W. Briggs V. E. Henson, S. McCormick. *A Multigrid Tutorial*, Society for Industrial and Applied Mathematics, (2000).

[3] F.J. Gaspar and J.L. Gracia and F.J. Lisbona. *Fourier analysis for multigrid methods on triangular grids.* SIAM J. Sci. Comput., 31 (2009), pp. 2081–2102.

[4] J.J. Heys, T.A. Manteuffel, S.F. McCormick, and L.N. Olson. *Algebraic multigrid for higher-order finite elements.* J. Comput. Phys., 204 (2005), pp. 520–532.

[5] M. Köster, and S. Turek. *The influence of higher order FEM discretisations on multigrid convergence.* Comput. Methods Appl. Math., 6 (2006), pp. 221–232.

[6] C.-C.J. Kuo and B.C. Levy. *Two-Color Fourier Analysis of the Multigrid Method with Red-Black Gauss-Seidel Smoothing.* Appl. Math. Comput., 29 (1989), pp. 69–87.

[7] S. Shu, D. Sun, J. Xu. *An algebraic multigrid method for higher-order finite element discretizations.* Computing, 77 (2006), pp. 347–377.

[8] U. Trottenberg, C.W. Oosterlee and A. Schüller. *Multigrid* Academic Press, New York, 2001.

[9] R. Wienands and W. Joppich. *Practical Fourier analysis for multigrid methods.* Chapman and Hall/CRC Press, 2005.